AIP | Journal of Applied Physics

Polyacrylonitrile nanofibers with added zeolitic imidazolate frameworks (ZIF-7) to enhance mechanical and thermal stability

Min Wook Lee, Seongpil An, Kyo Yong Song, Bhavana N. Joshi, Hong Seok Jo, Salem S. Al-Deyab, Sam S. Yoon, and Alexander L. Yarin

Citation: Journal of Applied Physics **118**, 245307 (2015); doi: 10.1063/1.4938112
View online: http://dx.doi.org/10.1063/1.4938112
View Table of Contents: http://scitation.aip.org/content/aip/journal/jap/118/24?ver=pdfcov
Published by the AIP Publishing

Polyacrylonitrile nanofibers with added zeolitic imidazolate frameworks (ZIF-7) to enhance mechanical and thermal stability

Min Wook Lee,[1,a)] Seongpil An,[2,a)] Kyo Yong Song,[2] Bhavana N. Joshi,[2] Hong Seok Jo,[2] Salem S. Al-Deyab,[3] Sam S. Yoon,[2,b)] and Alexander L. Yarin[1,2,b)]
[1]*Department of Mechanical and Industrial Engineering, University of Illinois at Chicago, 842 W. Taylor St., Chicago, Illinois 60607-7022, USA*
[2]*School of Mechanical Engineering, Korea University, Seoul 136-713, South Korea*
[3]*Department of Chemistry, King Saud University, Riyadh 11451, Saudi Arabia*

(Received 25 October 2015; accepted 5 December 2015; published online 31 December 2015)

Zeolitic imidazolate framework 7/polyacrylonitrile (ZIF-7/PAN) nanofiber mat of high porosity and surface area can be used as a flexible fibrous filtration membrane that is subjected to various modes of mechanical loading resulting in stresses and strains. Therefore, the stress-strain relation of ZIF-7/PAN nanofiber mats in the elastic and plastic regimes of deformation is of significant importance for numerous practical applications, including hydrogen storage, carbon dioxide capture, and molecular sensing. Here, we demonstrated the fabrication of ZIF-7/PAN nanofiber mats via electrospinning and report their mechanical properties measured in tensile tests covering the elastic and plastic domains. The effect of the mat fabrication temperature on the mechanical properties is elucidated. We showed the superior mechanical strength and thermal stability of the compound ZIF-7/PAN nanofiber mats in comparison with that of pure PAN nanofiber mats. Material characterization including scanning electron microscope, energy-dispersive X-ray spectroscopy, tensile tests, differential scanning calorimetry, and Fourier transform infrared spectroscopy revealed the enhanced chemical bonds of the ZIF-7/PAN complex.
[http://dx.doi.org/10.1063/1.4938112]

I. INTRODUCTION

Zeolitic imidazolate frameworks (ZIFs) are a class of metal organic frameworks (MOFs), which are composed of metal ions connected by organic ligands. ZIFs are crystalline nanoporous materials with features including high porosity, large surface area, and structural flexibility. They promise potential uses in H_2 storage, CO_2 capture, and molecular sensing applications.[1] Among various ZIFs, ZIF-7 was first discovered by Huang *et al*. in 2003.[2] The basic constitutive units of ZIF-7, Zn(II) metal ions bridged by benzimidazolate linkers, form a prototypical structure related to that of sodalite (SOD). The pore size of ZIF-7 is ~0.3 nm, which corresponds to the molecular sizes of H_2 (0.29 nm) and CO_2 (0.33 nm).[3] The two main synthesis approaches of *in situ* growth and secondary (seeded) growth on a porous support such as Al_2O_3 have been reported for the fabrication of ZIF-7 films and membranes.[4]

MOF-based materials have been used in gas separation applications.[5] However, filmization of MOF raw powder has been a challenge since requirements of the maximum surface-to-volume ratio and minimum inclusion of impurities in the film need to be satisfied. It would be desirable to implement these two requirements in the film fabrication process for the enhancement of gas adsorption and separation of MOF films.[6] In this spirit, MOF nanofibers (NFs) using compounds of MOF nanoparticles with polymers are in demand to fabricate highly permeable membranes with high mechanical strength and scalability for gas separation applications. MOF NFs could also overcome the limitations of handling MOF powders and their loss. Accordingly, MOF NFs can provide flexibility useful for the production of fibrous filters and membranes.[7,8] The electrospinning process is capable of producing polymer nanofibers on a massive scale for their use in membrane, biomedical, and optoelectronic applications. The nanoscale nature of electrospun fibers facilitates advantages of large surface-to-volume ratio, versatile surface functionalities, and superior mechanical strength when fibers are combined into a reinforced nanocomposite.[9] Electrospun ZIF NF mats with functionalized polymers may also possess an improved mechanical strength. In most applications, porous ZIFs are subjected to various modes of mechanical stress and strain. Hence, knowledge of the mechanical properties of ZIFs, such as their stress-strain dependences in the elastic and plastic regimes of deformation, is immensely important for practical applications. Unfortunately, few details are currently available regarding the mechanical characteristics of ZIFs and especially ZIF NFs.

According to the review by Tan and Cheetham, mechanical loading can generate tension, compression, shear, bending, and torsion in the ZIF and the effects of such loading define potential applications of the material.[10] In microelectromechanical system (MEMS)-based chemical sensing, microcantilevers coated with MOF films undergo stress. The MOF films must be stiff with good adhesion, and such mechanical properties of the material, as its elastic and plastic behavior, must be known for device design.[11] ZIFs used in gas sorption applications undergo hydrostatic compression;

[a)]M. W. Lee and A. An contributed equally to this work.
[b)]Authors to whom correspondence should be addressed. Electronic addresses: skyoon@korea.ac.kr and ayarin@uic.edu

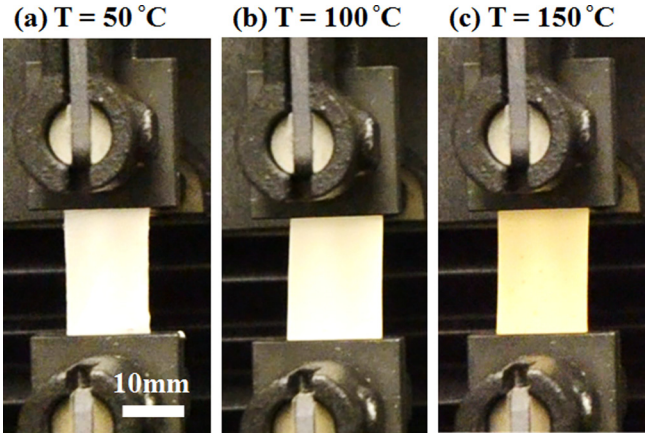

FIG. 1. Tensile tests of ZIF-7/PAN nanofiber mats synthesized at (a) T = 50 °C, (b) T = 100 °C, (c) T = 150 °C.

hence, they should possess high bulk and shear moduli to eliminate structural distortion, which could result in amorphization. Tan *et al*. reported that ZIF-8 has a relatively low shear modulus of 0.97 GPa,[12] indicating that the ZIF-8 structure can collapse upon the application of shear stresses. Following the study of Tan *et al*., Cao *et al*.[13] reported an experimental confirmation of rapid amorphization of ZIF-8 upon ball milling. Zhao *et al*. presented some results on the thermal stability of ZIF-7, reporting that the structure of ZIF-7 is stable at temperatures below 357 K, but above this temperature a phase transition occurs.[14] The structural rearrangement of the ZIF-7 crystalline structure was investigated by using Raman and X-ray diffraction (XRD) spectra.

In this context, a detailed study of the mechanical properties of MOF/ZIFs becomes extremely important. Tan *et al*. studied the single-crystal elastic constants of ZIF-8 by Brillouin scattering and nanoindentation along the three crystallographic axes of {100}/{110}/{111}; the reported Young's modulus values were in the 2.7–3.7 GPa range.[12] The mechanical properties of seven different ZIFs, characterized by single-crystal nanoindentation, were reported by Tan *et al*. and revealed Young's moduli and hardness values in the 3–10 GPa and 300 MPa–1.1 GPa ranges, respectively.[15] Notably, the elastic modulus of ZIF-7 is greater than that of ZIF-8. Accordingly, ZIF-7 is stiffer than ZIF-8 because of the sterically bulkier benzimidazolate present in ZIF-7. Very few studies have characterized the mechanical

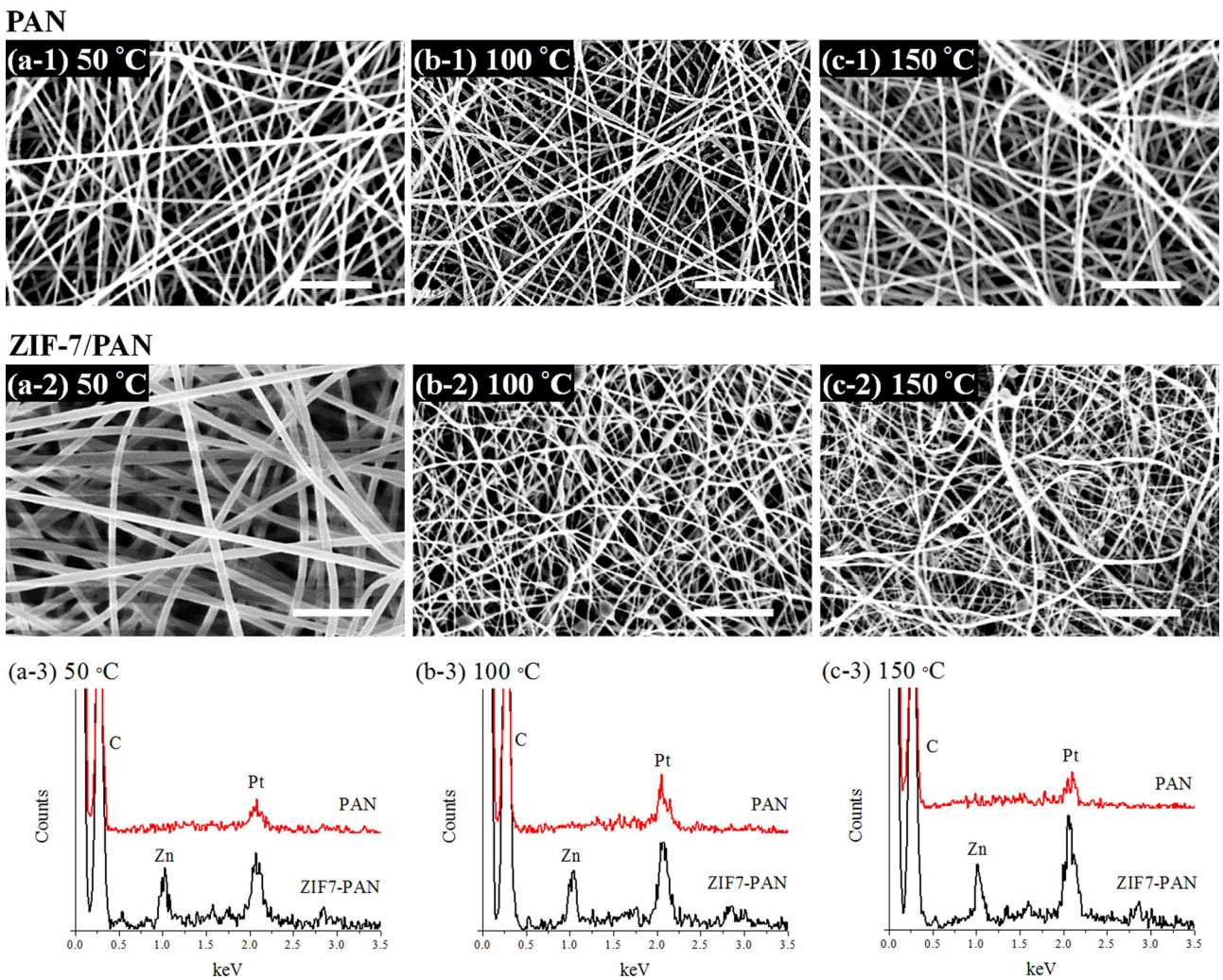

FIG. 2. SEM images of PAN ((a-1), (b-1), (c-1)) and ZIF-7/PAN ((a-2), (b-2), (c-2)) nanofibers, and EDX analyses of both ((a-3), (b-3), (c-3)) at different synthesis temperatures. Scale bar = 10 μm.

strength of ZIF/polymer compounds. MOF-mixed matrix membranes (MMM) were synthesized by Shashid *et al.* using ZIF-8 and Matrimid.[16] The Young's modulus of the MMM was increased with increasing the ZIF-8 content up to 30 wt. %. The increased Young's modulus indicated the enhanced interfacial adhesion between ZIF-8 nanoparticles and the polymer chains. ZIF-8 contents by more than 30% increased the membrane rigidity, thus decreasing its flexibility. Preparing 2D compact MOF structures such as films or membranes, care should be taken that the intrinsic mechanical properties, as well as the entire framework remain intact.

In the present study, we investigate the entire stress-strain dependence of ZIF-7/PAN NF mats. To the best of our knowledge, this is the first study on the mechanical properties of ZIF-7/PAN NF mats formed under different thermal conditions. The ZIF-7/PAN NFs were formed by electrospinning process.[17] The mechanical properties of the pristine PAN and ZIF-7/PAN NF mats were studied as explained in Secs. II and III.

II. EXPERIMENT

A. Materials and sample preparation

Prior to the preparation of the ZIF-7/PAN precursors for electrospinning and the ZIF-7 nanoparticles, zinc nitrate hexahydrate ($Zn(NO_3)_2{\cdot}6H_2O$, 98%), benzimidazole ($C_7H_6N_2$, 98%), PAN ($M_W = 150$ kDa), dimethylformamide (DMF, 99.8%), and methanol (99.8%) were purchased from Sigma-Aldrich. Preparation of solutions for electrospinning involved three stages. First, 8 wt. % zinc nitrate hexahydrate and 4 wt. % benzimidazole were dissolved separately in DMF. Second, these two solutions were mixed in a 1:1 weight ratio. Shortly afterward, 6 wt. % PAN solute was added to the mixed-solution to create the ZIF-7/PAN precursor for electrospinning. Third, to observe the effect of synthesis temperature, the precursor was stirred at different synthesis temperatures of T = 25 (room temperature, RT), 50, 100, and 150 °C for 3 days. After 3 days of synthesis, the obtained precursors were used to electrospin NF mats.[17,18] Pure PAN solutions used to form pure PAN nanofibers for comparison underwent similar

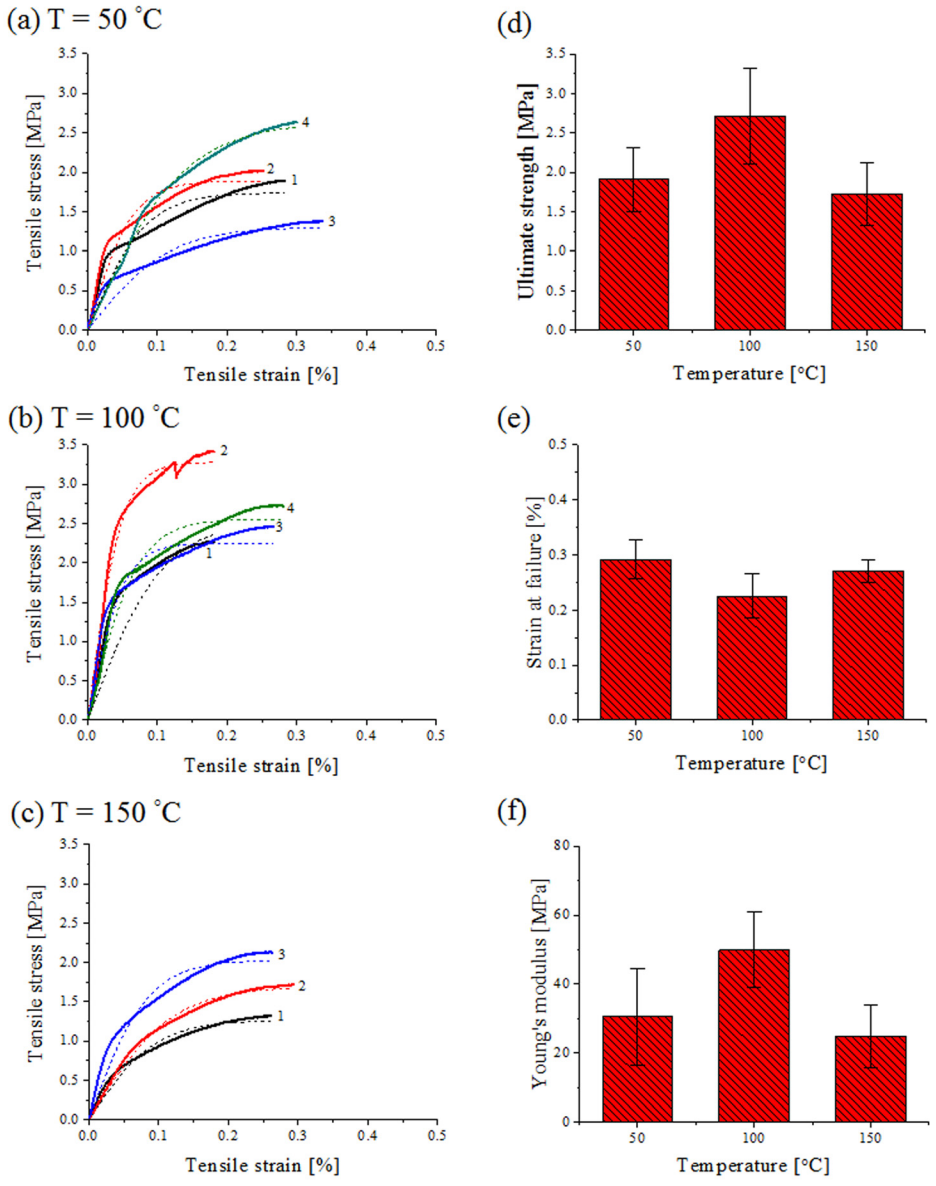

FIG. 3. Stress-strain curves of PAN nanofiber mats formed from solutions stirred at (a) T = 50 °C, (b) T = 100 °C, (c) T = 150 °C. (d) Ultimate strength. (e) Strain at failure. (f) Young's modulus. Strain rate = 10 mm/min. The experimental data are shown by solid curves with the numerals at the end being the trial number, the Green equation fitting-by the dashed curves.

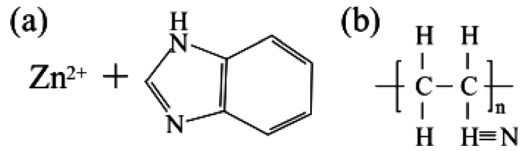

SCHEME 1. (a) ZIF-7; Zn(benzimidazole)$_2$,[19,20] (b) PAN; Polyacrylonitrile, $(C_3H_3N)_n$. $M_W = 150$ kDa, density $\rho = 1.184$ g/cm^3 at 25 °C, glass transition temperature $T_g = 85$ °C, melting temperature $T_m = 317$ °C.

stirring under these temperatures. The chemical structures of ZIF-7 and PAN are described schematically as Scheme 1. According to the thermogravimetric analyzer (TGA) data of our previous study (An *et al.*, ACS Sustainable Chem. & Eng., Submitted), 14.7% of the synthesized ZIF-NPs were embedded in the ZIF-7 PAN nanofibers at the synthesis temperature of 50 °C.

All solutions prepared under different temperatures were electrospun under identical conditions. A precursor was supplied through a stainless steel nozzle (18-gauge, EFD) using a syringe pump (Legato 100, KD Scientific Inc.) at a fixed flow rate of 150 μl/h. To form a stable Taylor cone, a high voltage in the range of 7–9 kV was applied by a power supply (EP20P2, Glassman High Voltage Inc.). Two syringes and a drum collector were used to fabricate large-size NF mats. The nozzle-to-collector distance was fixed at 7 cm.

B. Tensile tests

The prepared nanofiber mats were cut in 15×60 mm^2 pieces and clamped with two pneumatic grips spaced 20 mm apart. An Instron 5942 with a 100 N load cell stretched the samples at rates of 1 and 10 mm/min until the samples were completely fractured. Each test was repeated three to five times for each sample synthesized under different temperature and the averaged results of each case are reported below. Typical samples used in tensile tests are shown in Fig. 1.

C. Characterization

Micro-images and elemental analyses were obtained by scanning electron microscopy with energy dispersive X-ray spectroscopy (SEM/EDS, Hitachi S-3000 N), and transmission electron microscope (TEM) images were taken (JEM

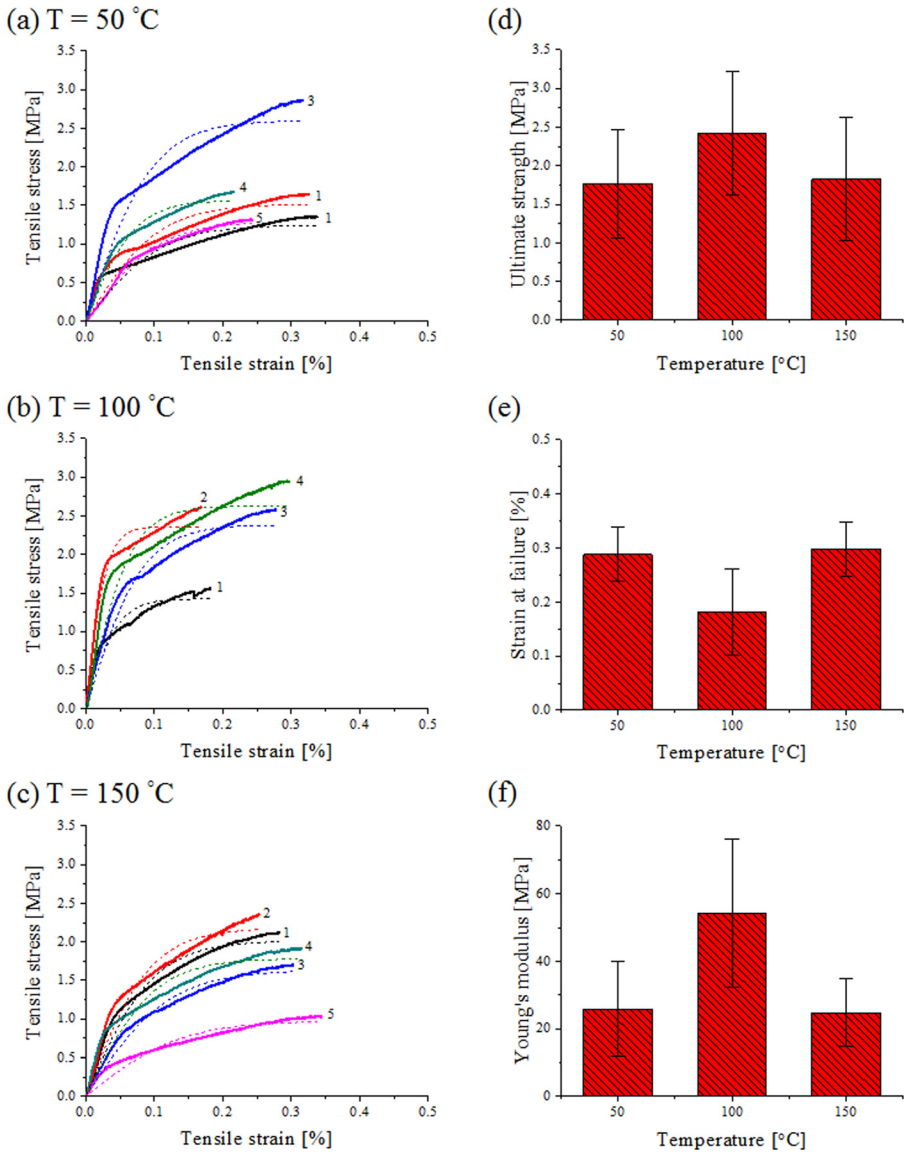

FIG. 4. Stress-strain curves of PAN nanofiber mats formed from solutions stirred at (a) T = 50 °C, (b) T = 100 °C, (c) T = 150 °C. (d) Ultimate strength. (e) Strain at failure. (f) Young's modulus. Strain rate = 1 mm/min. The experimental data are shown by solid curves with the numerals at the end being the trial number, the Green equation fitting-by the dashed curves.

2100F, JEOL Inc.) at 200 kV. Fourier transform infrared spectroscopy (FT-IR) was performed [Horiba LabRam Aramis IR2; 64 scans at a resolution of 8 cm^{-1} in the spectral range of 4000–720 cm^{-1} in attenuated total reflectance (ATR) mode] to reveal the structural information of the prepared nanofiber mat samples. Thermograms were obtained by differential scanning calorimetry (DSC, 8500 Isothermal) under flowing N_2 at a rate of 20.0 ml/min from 25.0 °C to 450.0 °C with temperature variation at the rate of 5.0 °C/min.

III. RESULTS AND DISCUSSION

A. Observations

As seen in Fig. 1, the sample color changes from white to yellow as the synthesis temperature T increases from 50 to 100 to 150 °C because of the heated PAN component in the fibers.[21] The results of the morphological and elemental analyses obtained by SEM and EDX, respectively, are shown in Fig. 2. The PAN fiber diameter is 567 ± 110, 453 ± 99, and 558 ± 124 nm for T = 50, 100, and 150 °C, respectively. The diameter of the ZIF-7/PAN fiber is 1208 ± 925 nm, 404 ± 150 nm, and 350 ± 131 nm for T = 50, 100, and 150 °C, respectively. The EDX spectra reveal clear peaks at 1.01 keV corresponding to the presence of Zn in all the three cases of ZIF-7/PAN NFs [see Figs. 2(a)–2(c)].

B. Results of tensile tests

The tensile test results at strain rates of 10 and 1 mm/min for the PAN and ZIF-7/PAN nanofiber mats are shown in Figs. 3–6. The experimental stress-strain curves (solid lines) from the tensile tests are compared with the elasto-plastic Green equation discussed in Section III C (dashed lines) in panels (a)–(c) of each figure. The stress-strain curves of the PAN nanofiber mats in Figs. 3 and 4 indicate temperature dependence of mechanical characteristics. The temperature range covered includes the glass transition temperature of PAN ($T_g \sim 85$ °C) and the temperature T = 150 °C, well above T_g, at which the semi-crystalline PAN nanofiber become rubber-like and the strength and stiffness (Young's modulus) decline.

ZIF-7/PAN NF samples were synthesized at T = 50, 100, and 150 °C and then used in tensile tests. Figs. 5 and 6

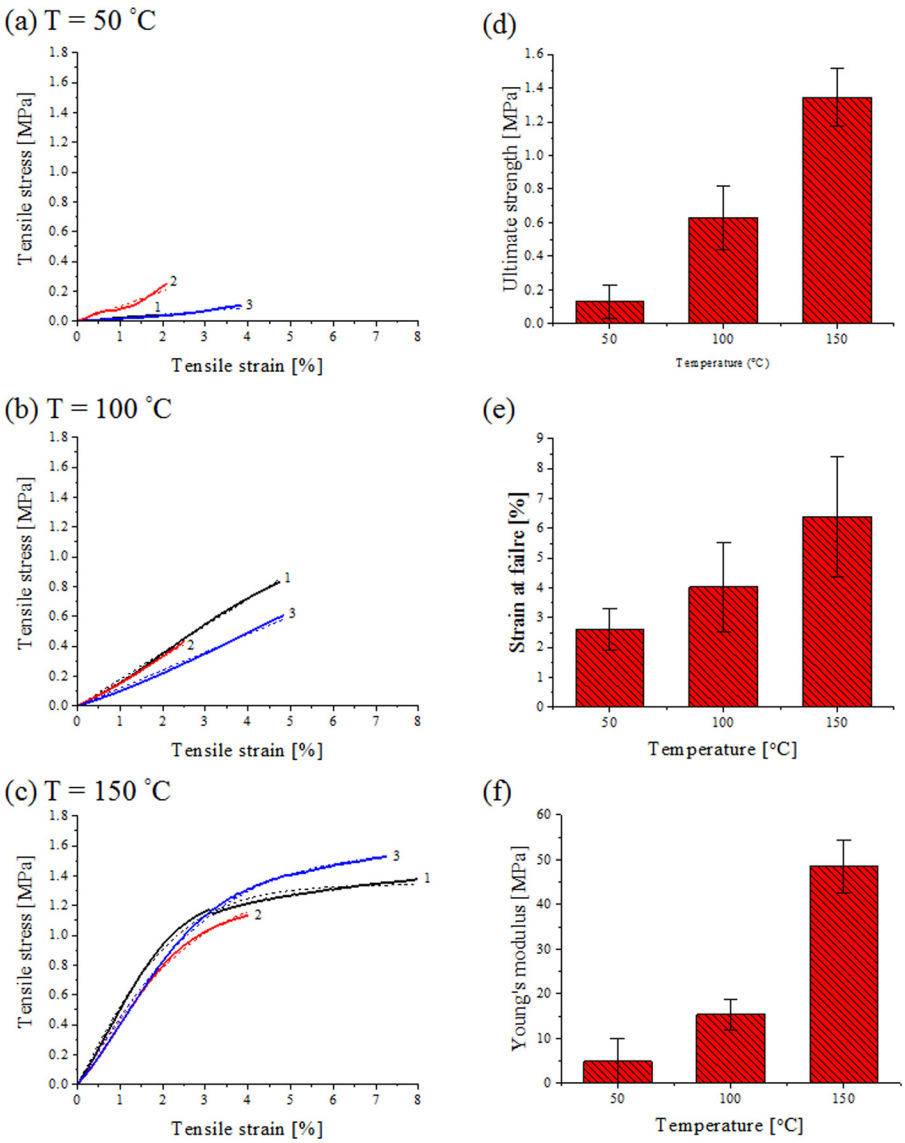

FIG. 5. Stress-strain curves of ZIF-7/PAN nanofiber mats synthesized at (a) T = 50 °C, (b) T = 100 °C, (c) T = 150 °C. (d) Ultimate strength. (e) Strain at failure. (f) Young's modulus. Strain rate = 10 mm/min. The experimental data are shown by solid curves with the numerals at the end being the trial number, the Green equation fitting-by the dashed curves.

depict the stress-strain curves of the ZIF-7/PAN NF mats synthesized at T = 50, 100, and 150 °C and tested at stretching rates of 10 and 1 mm/min. The stress-strain curves in panel (a) are similar to that of the PAN fiber mats reported before.[22] The ultimate strength and strain at failure and Young's modulus continuously increase beyond the glass transition temperature of PAN. The stress-strain curves at T = 100 °C in panel (b) reveal a catastrophic failure after the elastic region, while those at T = 150 °C in panel (c) reveal a plastic region following the elastic region. Notably, the plasticity first appears in samples synthesized at T = 150 °C. The plastic metal-like behavior of the ZIF-7/PAN nanofiber mats is shown in panel (c). The fit of the theoretical curve corresponding to the elastic-plastic behavior of metals to the experimental results for the ZIF-7/PAN samples reveals metal-like plasticity of ZIF-7/PAN NFs (the fitting accuracy is 99% in these cases). As the synthesis temperature increases from 50 to 150 °C, the fiber mat stiffness (Young's modulus) increases. Synthesis at T > 100 °C provides higher stiffness in the low-strain domain followed by ductility in the high-strain domain. Notably, the strength and stiffness are enhanced at higher preparation temperatures, which is the opposite of the performance of pure polymer nanofiber mats.

The mechanical properties are summarized in Fig. 7 for the comparison of different heat treatment and strain rates. As the heating temperature increases, PAN the strength and stiffness are diminished at the highest temperature of 150 °C, however, ZIF-7/PAN they keep increasing at with temperature. The effect of ZIF-7 in PAN fibers enhances thermal stability and mechanical properties even beyond the glass transition temperature of PAN. The strain rate does not show any significant impact on the mechanical properties tested at stretching rates of 10 or 1 mm/min for PAN. However, in the case of ZIF-7/PAN (especially at the stretching rate of 1 mm/min; black lines in Fig. 7), the strength and stiffness increase with temperature is visibly different from those measured at 10 mm/min (red lines in Fig. 7).

C. Discussion of the results of tensile tests

It should be emphasized that the data in Figs. 3–6 reveal that reproducibility of the entire stress-strain curve in several cases is rather pure, with the elastic part being much better

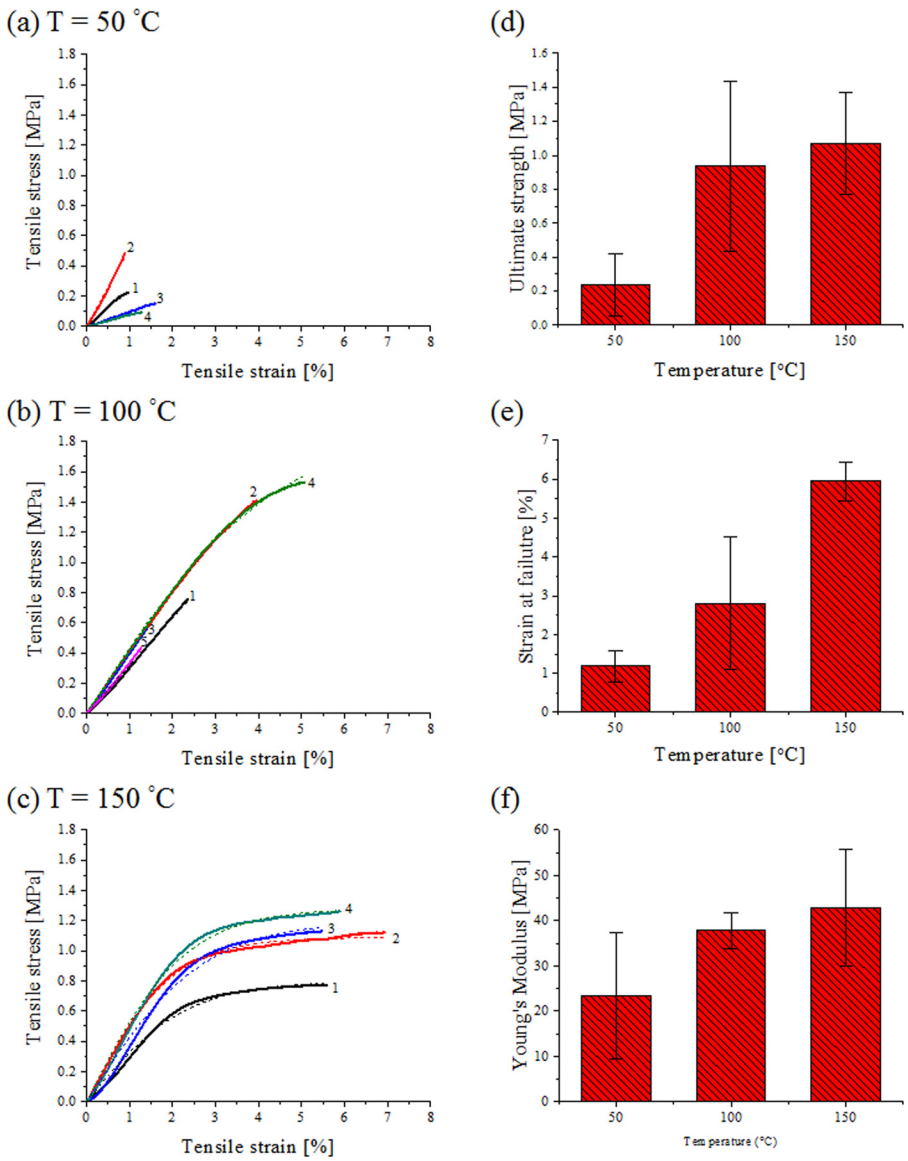

FIG. 6. Stress-strain curves of ZIF-7/PAN nanofiber mats synthesized at (a) T = 50 °C, (b) T = 100 °C, (c) T = 150 °C. (d) Ultimate strength. (e) Strain at failure. (f) Young's modulus. Strain rate = 1 mm/min. The experimental data are shown by solid curves with the numerals at the end being the trial number, the Green equation fitting-by the dashed curves.

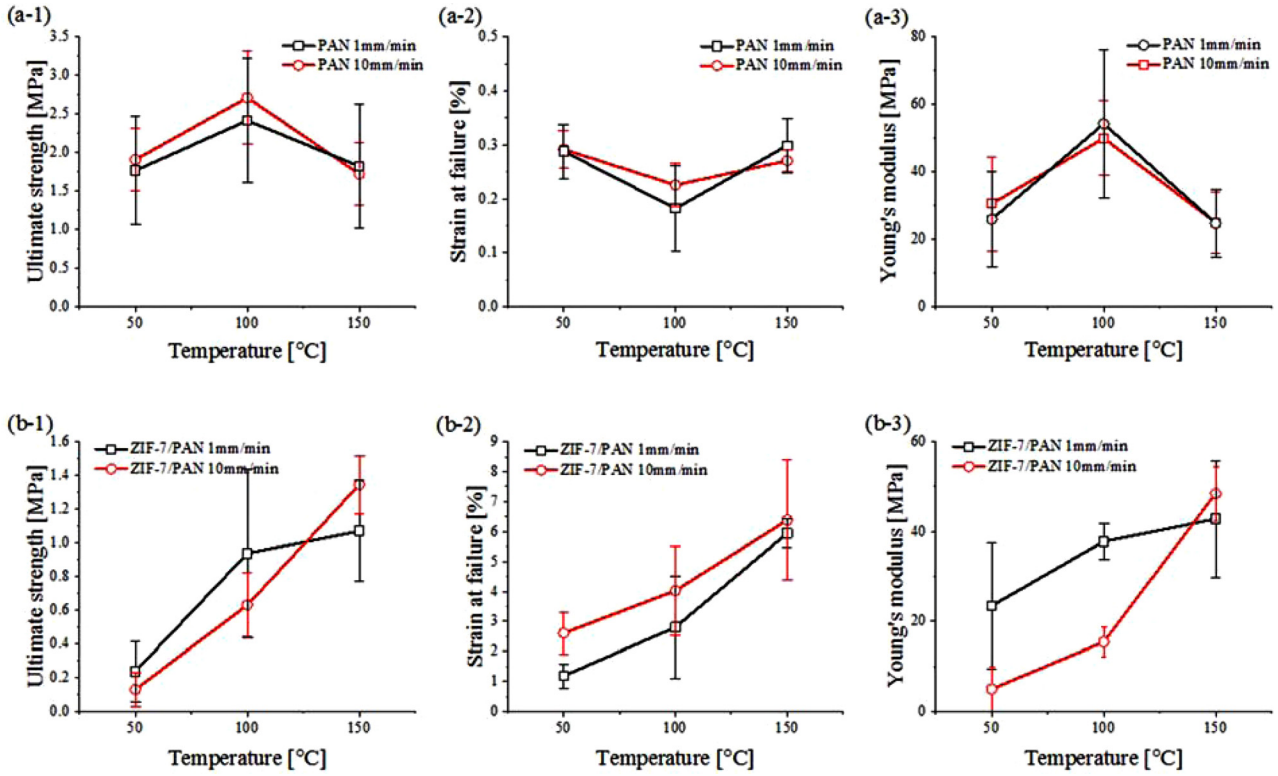

FIG. 7. Mechanical properties versus heat treatment temperature and strain rate. (a) PAN nanofiber mat. (b) ZIF-7/PAN nanofiber mat. (Panels 1) Ultimate strength. (Panels 2) Strain at failure. (Panels 3) Young's modulus.

reproducible than the plastic one. To obtain the mechanical properties from the stress-strain curves spanning the elastic and plastic domains, the elastic-plastic Green equation[23,24] is frequently used

$$\sigma_{xx} = Y\tanh\left(\frac{E}{Y}\varepsilon\right), \tag{1}$$

where σ_{xx} is the tensile stress, E is Young's modulus, Y is the yield stress, and ε is the tensile strain.

This phenomenological equation describes a gradual transition from the elastic to the plastic domain.[23,25] Eq. (1) was fitted to the experimental stress-strain curves measured for the ZIF-7/PAN nanofiber mats in Figs. 5 and 6 and the corresponding values of the mechanical parameters are listed in Table I. The yield stress values are listed only in those cases where the Green equation could fit the plastic domain sufficiently accurately. It should be emphasized that Green's equation (1) implies elastic-perfectly plastic transition, which was not the case in Figs. 3 and 4 (PAN nanofiber mats). The agreement with Eq. (1) was much better in Figs. 5 and 6 (ZIF-7/PAN nanofiber mats). However, Eq. (1) would also fail when a yield plateau was not present at all or a sample would break prematurely (in some cases in Figs. 5 and 6. When Green's equation was capable of fitting the data in Figs. 5 and 6, the fitting revealed the accuracy of 99%.

D. Thermal analysis

In addition, the material properties of the ZIF-7/PAN NF mats studied in the tensile tests were analyze during DSC. In the previously published differential thermogravimetry (DTG) results, degradation of pure PAN nanofibers began to occur at ~85 °C, which is the glass transition temperature of PAN.[17] However, the results of the present work show that ZIF-7/PAN nanofibers reveal no thermal degradation in this

TABLE I. Mechanical parameters measured experimentally as revealed by the Green equation (1).

Case	Strain rate [mm/min]	Synthesis temperature [°C]	Young's modulus, E [MPa]	Yield stress, Y [MPa]
			25.140	0.056
Figure 5(a)	10	50	10.094	–
			23.370	–
			17.878	–
Figure 5(b)	10	100	16.402	–
			12.003	–
			54.973	1.345
Figure 5(c)	10	150	44.472	1.332
			46.004	1.570
			25.732	0.502
Figure 6(a)	1	50	51.163	–
			9.545	–
			7.527	0.760
			31.515	–
			41.414	2.436
Figure 6(b)	1	100	39.373	–
			43.893	1.915
			32.933	–
			34.471	0.797
Figure 6(c)	1	150	54.432	1.090
			44.407	1.195
			55.928	1.281

domain, i.e., the compounding of PAN with ZIF-7 enhances thermal stability at the glass transition temperature of PAN.

Fig. 8(a) shows the DSC curves of the PAN (solid line) and ZIF-7/PAN (dashed line) nanofiber mats. The results for the samples synthesized at T = RT, 50, 100, and 150 °C are depicted by black, red, green, and blue lines, respectively. The thermograms in Figs. 8(b) and 8(c) detail the phase-change domains for PAN and ZIF-7/PAN, respectively. The endothermic peak temperature T_m (the melting temperature) of the PAN fiber mat is ~293 °C. It should be emphasized that the melting temperature increases for ZIF-7/PAN as the synthesis temperature increases panel (c). The peak temperature depends strongly on the degree of crystallinity or the crystal size of the material.[26] The delay in melting for the compound nanofibers demonstrates that the combination of ZIF-7 and PAN provides an extra thermal stability to the material. As shown in Fig. 8(d), the melting temperature T_m of ZIF-7/PAN increases as the synthesis temperature increases from 50 to 100 and 150 °C, while that of PAN decreases. The melting temperature of ZIF-7/PAN is by ~10 °C higher than that of PAN stirred at T = 150 °C.

It should be emphasized that the melting enthalpy of PAN decreases as the temperature at which the solution was stirred had been increased, Fig. 8(b). This probably stems from the fact that at higher solution preparation temperatures PAN undergoes thermal degradation to a certain degree. On the other hand, ZIF-7/PAN metalorganic compounds synthesized at different temperatures do not reveal any trend in melting enthalpy as the preparation temperature increases, Fig. 8(c). The latter probably points at a competition of partial thermal degradation of PAN and stronger bonds in metalorganic compounds formed at higher temperatures. As discussed in Section III C, the ZIF-7/PAN mats revealed an enhanced ductility and strength reduction compared to the PAN mats. Moreover, lower crystallinity (and lower enthalpy) is expected for ZIF-7/PAN specimens as seen in Fig. 8. It is probably due to the limited chain mobility caused by the addition of ZIF-7. The amorphous phase due to the presence of ZIF-7 in PAN results in higher ductility up to much higher strains at failure than for pure PAN (see Fig. 7(a-2) and 7(b-2)).

E. IR spectra

In Fig. 9, PAN and ZIF-7 nanofiber samples are identified by the peaks at 2245 and 1454 cm^{-1} and 1301, 1253, and 749 cm^{-1}, respectively.[19,20,27,28] PAN and ZIF-7 are easily distinguished in the compound ZIF-7/PAN sample. The low-wavenumber domain of the spectrum [cf. Fig. 9(b)] for ZIF-7/PAN nanofibers is detailed in Figs. 9(c)–9(f). In panel (c), the peak at 1482 cm^{-1} experiences a blue shift to 1470 cm^{-1} as the synthesis temperature rises from 50 to 150 °C. The peak is attributed to C=C stretching at 1400–1600 cm^{-1}. Similar blue

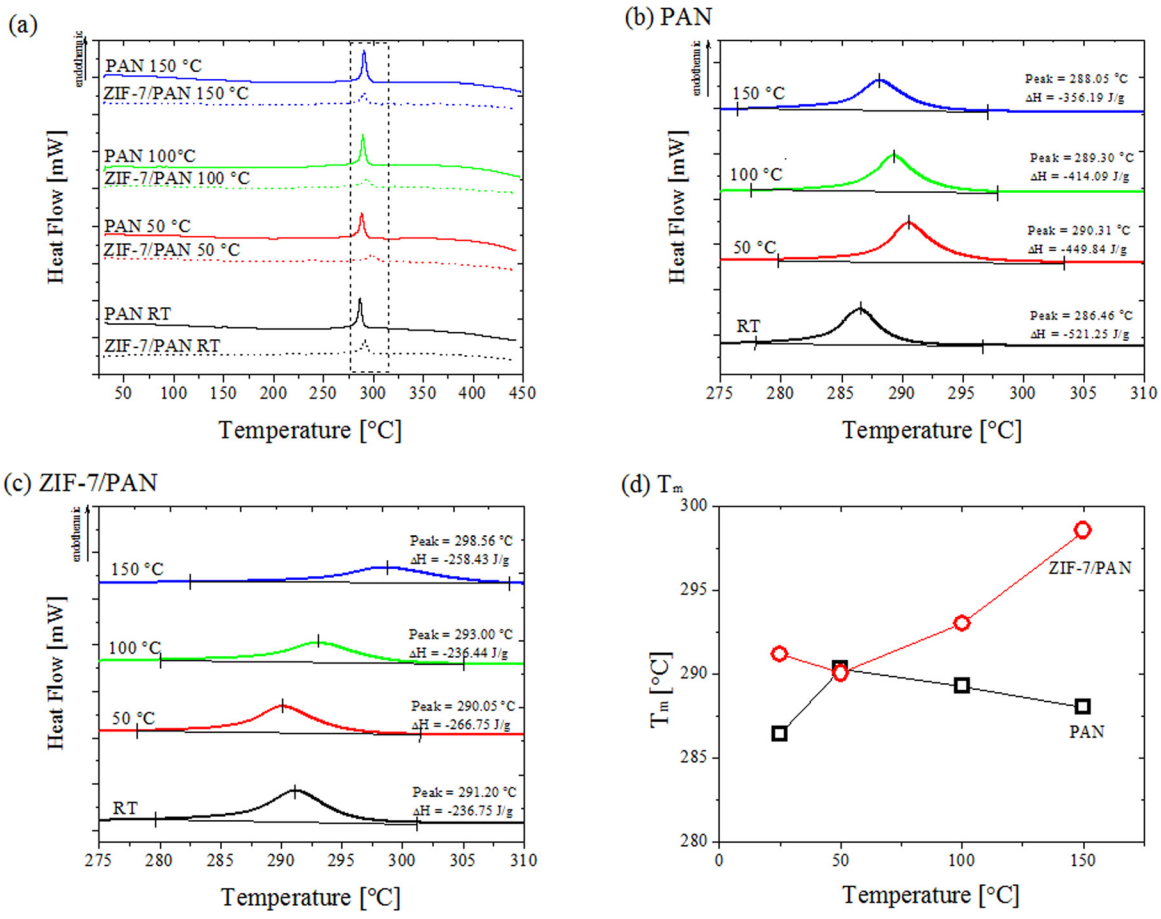

FIG. 8. DSC thermogram (a) Full temperature range. (b) The range around the melting temperature of PAN. (c) The range around the melting temperature of ZIF-7/PAN. (d) Comparison of the melting temperatures of PAN and ZIF-7/PAN.

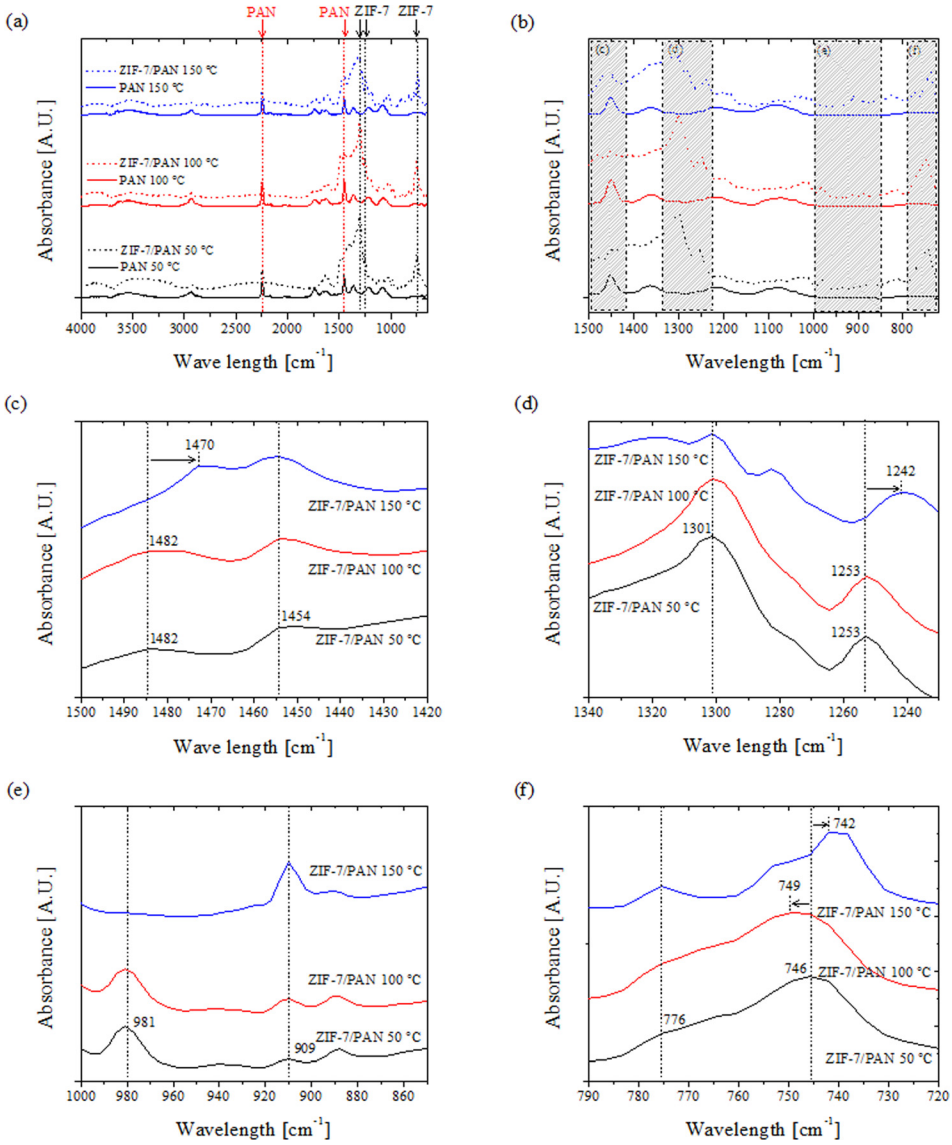

FIG. 9. FT-IR spectra (a) Full wavelength range (4000–720 cm^{-1}). (b) Zoom-in of the 1500–720 cm^{-1} range, (c) of the 1500–1420 cm^{-1} range, (d) of the 1340–1230 cm^{-1} range, (e) of the 1000–850 cm^{-1} range, and (f) of the 790–720 cm^{-1} range.

shifts occur for the peaks located at 1253 and 746 cm^{-1}, assigned to C-N stretching and C-H bending, respectively, in panels (d) and (f). As is well-known, stronger bonds in the molecular structure require higher energies to experience vibration under IR radiation; hence, the frequency increases and the wavenumber decreases. In panel (e), the intensity of the peak at 909 cm^{-1}, corresponding to C=C bending, increases for the sample synthesized at 150 °C. The C=C, C-N, and C-H bonds correlate to the main structure of the ZIF-7/PAN NF. Strengthening of the NF backbone causes the increased strength of the nanofiber mat at increased synthesis temperatures. Notably, the strengthening effect of each bond occurs in the ZIF-7/PAN compound nanofibers, but not in the PAN nanofiber mat. The PAN nanofiber mat deteriorated in strength and stiffness at the stirring temperature of 150 °C, as shown in Figs. 3 and 4. Above the glass transition temperature of PAN, the heat treatment weakens the PAN nanofiber mats. However, the combination of PAN and ZIF-7 creates a new stable structure that becomes stronger and more durable at higher synthesis temperatures, reflecting the mechanical and thermal stability of the compound nanofibers.

IV. CONCLUSIONS

The blends of ZIF-7 and PAN prepared at different synthesis temperatures of 50, 100, and 150 °C were used to electrospin nanofiber mats and to compare them with nanofiber mats electrospun from pure PAN. It was found that the diameter of both ZIF-7/PAN and pure PAN nanofibers decreased as the synthesis temperature increased. The tensile test revealed that the strength and stiffness of the electrospun ZIF-7/PAN nanofiber mats increased when the synthesis temperature at the solution preparation stage was higher. Also, ZIF-7/PAN nanofiber mats revealed significant plasticity reminding that of metals and being in good agreement with the predictions of the elastic-plastic Green equation. The DSC thermogram showed that the melting temperature of ZIF-7/PAN increased at higher temperatures at the solution preparation stage. On the contrary, the PAN nanofiber

mats revealed exactly the opposite trend. At the highest solution preparation temperature of T = 150 °C, the melting temperature of ZIF-7/PAN nanofibers was higher than that of PAN nanofibers by 10 °C. The modified mechanical properties and higher thermal stability of ZIF-7/PAN nanofibers in comparison to pure PAN nanofibers are attributed to the blue shift of the peaks for C=C, C-N, and C-H bonds in the infrared spectra in the case of high synthesis temperature at the solution preparation stage (T = 150 °C).

ACKNOWLEDGMENTS

This research was supported by Global Frontier Program through the Global Frontier Hybrid Interface Materials (GFHIM) of the National Research Foundation of Korea (NRF) funded by the Ministry of Science, ICT & Future Planning (2013M3A6B1078879), NRF-2013R1A2A2A050 05589, KETEP-20133030010890, and the Industrial Strategic Technology Development Program (10045221). The authors extend their appreciation to the Deanship of Scientific Research at King Saud University for its funding this Prolific Research group (PRG-1436-03).

[1]P. Zhao, T. D. Bennett, N. P. M. Casati, G. I. Lampronti, S. A. Moggach, and S. A. T. Redfern, Dalton Trans. **44**, 4498 (2015).
[2]X. Huang, J. Zhang, and X. Chen, Chin. Sci. Bull. **48**, 1531 (2003).
[3]Y. Li, F. Liang, H. Bux, W. Yang, and J. Caroa, J. Membr. Sci. **354**, 48 (2010).
[4]L. Fan, M. Xue, Z. Kang, H. Li, and S. Qiu, J. Mater. Chem. **22**, 25272 (2012).
[5]M. J. C. Ordonez, K. J. Balkus, J. P. Ferraris, and I. H. Musselman, J. Membr. Sci. **361**, 28 (2010).
[6]J. A. Mason, M. Veenstra, and J. R. Long, Chem. Sci. **5**, 32 (2014).
[7]P. Silva, S. M. F. Vilela, J. P. C. Tome, and F. A. A. Paz, Chem. Soc. Rev. **77**, 6774 (2015).
[8]M. Rose, B. Bohringer, M. Jolly, R. Fischer, and S. Kaskel, Adv. Eng. Mater. **13**, 356 (2011).
[9]Z.-M. Huang, Y.-Z. Zhang, M. Kotaki, and S. Ramakrishna, Compos. Sci. Technol. **63**, 2223 (2003).
[10]J. C. Tan and A. K. Cheetham, Chem. Soc. Rev. **40**, 1059 (2011).
[11]B. V. d. Voorde, R. Ameloot, I. Stassen, M. Everaert, D. D. Vos, and J.-C. Tan, J. Mater. Chem. C **1**, 7716 (2013).
[12]J.-C. Tan, B. Civalleri, C.-C. Lin, L. Valenzano, R. Galvelis, P.-F. Chen, T. D. Bennett, C. Mellot-Draznieks, C. M. Zicovich-Wilson, and A. K. Cheetham, Phys. Rev. Lett. **108**, 095502 (2012).
[13]S. Cao, T. D. Bennett, D. A. Keen, A. L. Goodwind, and A. K. Cheetham, Chem. Commun. **48**, 7805 (2012).
[14]P. Zhao, G. I. Lampronti, G. O. Lloyd, M. T. Wharmby, S. Facq, A. K. Cheetham, and S. A. T. Redfern, Chem. Mater. **26**, 1767–1769 (2014).
[15]J. C. Tan, T. D. Bennett, and A. K. Cheetham, Proc. Natl. Acad. Sci. U.S.A. **107**, 9938 (2010).
[16]S. Shahid, K. Nijmeijer, S. Nehache, I. Vankelecom, A. Deratani, and D. Quemener, J. Membr. Sci. **492**, 21 (2015).
[17]S. An, J. S. Lee, B. N. Joshi, H. S. Jo, K. Titov, J.-S. Chang, C.-H. Jun, S. Al-Deyab, Y. K. Hwang, J.-C. Tan, and S. S. Yoon, "Zeolitic imidazolate framework-7nanocomposite fibers synthesized by electrospinning and their potential application in CO_2 capture," ACS Sustainable Chem. & Eng. (submitted).
[18]A. L. Yarin, B. Pourdeyhimi, and S. Ramakrishna, *Fundamentals and Applications of Micro- and Nanofibers* (Cambridge University Press, Cambridge, 2014).
[19]Y. Ying, Y. Xiao, J. Ma, X. Guo, H. Huang, Q. Yang, D. Liu, and C. Zhong, RSC Adv. **5**, 28394 (2015).
[20]T. Yang, Y. Xiao, and T.-S. Chung, Energy Environ. Sci. **4**, 4171 (2011).
[21]S. Lee, J. Kim, B.-C. Ku, J. Kim, and H.-I. Joh, Adv. Chem. Eng. Sci. **2**, 275 (2012).
[22]M. W. Lee, S. An, H. S. Jo, S. S. Yoon, and A. L. Yarin, ACS Appl. Mater. Interfaces **7**, 19546 (2015).
[23]A. E. Green, Proc. R. Soc. London, Ser. A **234**, 46 (1956).
[24]S. Khansari, S. Sinha-Ray, A. L. Yarin, and B. Pourdeyhimi, J. Appl. Phys. **111**, 044906 (2012).
[25]W. Prager, J. Appl. Phys. **19**, 540 (1948).
[26]A. El-Hadi, R. Schnabel, E. Straube, G. Müller, and S. Henning, Polym. Test. **21**, 665 (2002).
[27]F. Nacimiento, R. Alcantara, J. R. Gonzalez, and J. L. Tirado, J. Electrochem. Soc. **159**, A1028 (2012).
[28]F. Li, Q. Li, X. Bao, J. Gui, and X. Yu, Korean Chem. Eng. Res. **52**, 340 (2014).